

LABORATORY STUDY OF DYNAMIC FRACTURE IN PRE-DRILLED BOREHOLES AND ASSOCIATED HOST ROCK BEHAVIOUR

CHENG GUO ZHANG

*College of Energy and Mining Engineering, Shandong University of Science and Technology, Qingdao, China, and
State Key Laboratory of Mining Disaster Prevention and Control Co-founded by Shandong Province and the Ministry
of Science and Technology, Shandong University of Science and Technology, Qingdao, China*

XUEBIN GU

College of Energy and Mining Engineering, Shandong University of Science and Technology, Qingdao, China

WEIYAO GUO

*College of Energy and Mining Engineering, Shandong University of Science and Technology, Qingdao, China, and
State Key Laboratory of Mining Disaster Prevention and Control Co-founded by Shandong Province and the Ministry
of Science and Technology, Shandong University of Science and Technology, Qingdao, China, and
Graduate School of Engineering, Nagasaki University, Nagasaki, Japan
corresponding authors Weiyao Guo, e-mail: 363216782@qq.com*

XUFEI GONG

*College of Energy and Mining Engineering, Shandong University of Science and Technology, Qingdao, China, and
State Key Laboratory of Mining Disaster Prevention and Control Co-founded by Shandong Province and the Ministry
of Science and Technology, Shandong University of Science and Technology, Qingdao, China*

HENGYU FANG

College of Energy and Mining Engineering, Shandong University of Science and Technology, Qingdao, China

HE HUANG

Nantun Coal Mine, Yankuang Energy Group Co., Ltd., Jining, China

To better understand the influence of the openings and their relationship with the host rock, laboratory tests were conducted on a range of sandstone specimens with different proportions of D/H (hole diameter/specimen height) ratio. Acoustic emission (AE) and video monitoring were used to capture the rock specimen responses. The results showed that if the D/H ratio was less than 0.3, the fracture mode occurred in the hole, indicating that this was an appropriate ratio. In addition, the “short quiet period” of AE energy can be used as a precursor for determining the burst in the opening.

Keywords: rock burst, pre-drilled hole, size ratio, acoustic emission

1. Introduction

The rock burst is one of the most challenging topics in underground excavation projects, particularly under high stress. It often occurs suddenly and is accompanied by violent rock ejection, which seriously threatens safety and productivity (Zhao *et al.*, 2021; Chen *et al.*, 2022; Zhang *et al.*, 2022). To study the mechanism of rock burst, many extensive researches were conducted in the literature previously, using methodologies including numerical simulation (Baranowski *et al.*, 2022), analytical analysis (Kucewicz *et al.*, 2023) and laboratory tests (Farhadian, 2021). Among them, laboratory testing on rock specimens in various conditions are a common method to establish the first understanding of rock behaviour under different types of loading.

In the rock burst related laboratory testing, uniaxial, biaxial and triaxial are common loading types used to specimens (Huang *et al.*, 2022; Liu *et al.*, 2021). In particular, the relationship between rock failure and acoustic emission characteristics are studied for identifying fracture and energy release mechanisms (Dong *et al.*, 2021; Chen *et al.*, 2023). For example, there are studies on the rock unit near the excavation opening to examine the relationship between the stress gradient, loading rate and temperature and the deformation (Su *et al.*, 2017, 2019). Faradonbeh *et al.* (2020) established a comprehensive database of true-triaxial unloading tests on rocks with a wide range of properties. He *et al.* (2012) adopted a self-developed triaxial loading system to study the role of confinement to rock burst initiation in different types of rock.

Another group of tests is focused on the borehole behaviour in a rock block under different types of loading, simulating the rock burst condition in the holes. In those tests, the excavations and nearby rock were mainly simplified into small-sized specimens to study failure laws of the opening during the loading process. The effect of the opening shape have also been studied in the literature. For example, in non-circular cavity research, Wu *et al.* (2019) studied failure characteristics of *U*-shaped cavities under a uniaxial loading. Luo *et al.* (2019) studied failure characteristics of the *D*-shaped cavity under the true triaxial loading. In research on circular openings, Hu *et al.* (2019) and Liang *et al.* (2019) studied the biaxial loading of circular caverns, mainly discussing the laws of the acoustic emission and rock burst. Zhang *et al.* (2016) explored the impact of lateral stress on rock bursts in circular caverns under a biaxial loading. Si *et al.* (2018) and Gong *et al.* (2017) studied the rock burst process and failure characteristics of circular caverns under the true triaxial loading.

Apart from the shape of excavations, in small-scale laboratory experimental research, the size effect is a critical factor. For example, Martin (1997) found that as the borehole size increases, the tangential stress at failure approaches the unconfined compressive strength of the material but a significant strength-scale effect is observed for boreholes less than 75 mm in diameter. The ratio of the hole diameter to the specimens size (i.e. size ratio) is closely related to the test results, and it is not fully studied in the previous studies. Therefore, uniaxial loading tests were performed on sandstone specimens with different scales of D/H , while AE and video monitoring were used to capture the response of the rock specimens. The findings of this study are expected to provide a reference for determining the extent of failure of underground openings.

2. Specimen preparation and test setup

2.1. Specimen preparation

Green sandstone samples with uniform texture were selected from a mine site in Shandong Province in China for tests. The material was processed into five specimens with circular holes (30 mm in diameter) according to ISRM's requirements, as shown in Fig. 1 and Table 1. Measuring mechanical parameters, the uniaxial compressive strength was equal to 82 MPa, the elastic modulus has reached 12.8 GPa. The scanning electron microscope (SEM) results show that sandstone has a dense cementation structure with fewer intergranular pores and fissures, indicating that the sandstone has good homogeneity, as shown in Fig. 1c. The five specimens are classified *A-E* according to the D/H ratio (i.e. hole diameter/height), as shown in Table 1.

2.2. Test system setup

The experimental system, shown in Fig. 2a, consists of the following three parts: loading equipment (RLJW-2000 servo rock-testing machine), an acoustic emission instrument (AMSY-6 acoustic emission detection system produced by Vallen, Germany), and a visual observation system (EOS C100 camera). During the test, two acoustic emission sensors were arranged on

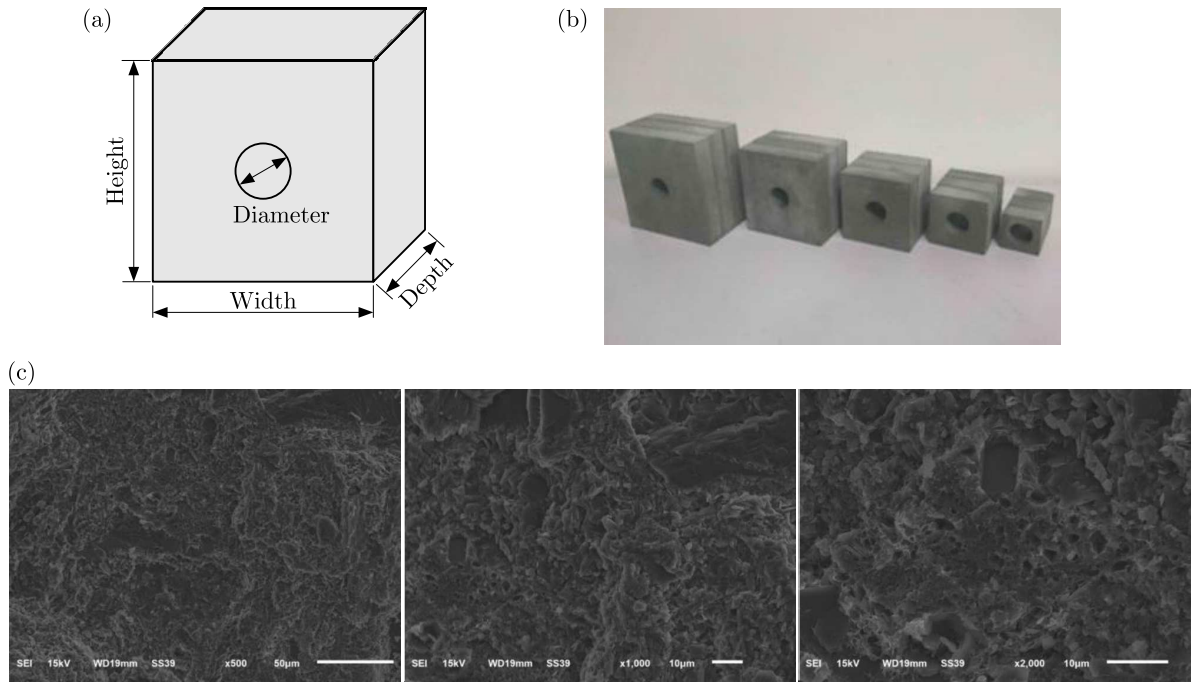


Fig. 1. (a) Geometrical features of the specimen, (b) manufactured specimens and (c) microscopic feature

Table 1. Dimensions of specimens

Type	Height H [mm]	Depth [mm]	Diameter D [mm]	D/H
A	50	30	30	0.6
B	75	30	30	0.4
C	100	30	30	0.3
D	125	30	30	0.24
E	150	30	30	0.2

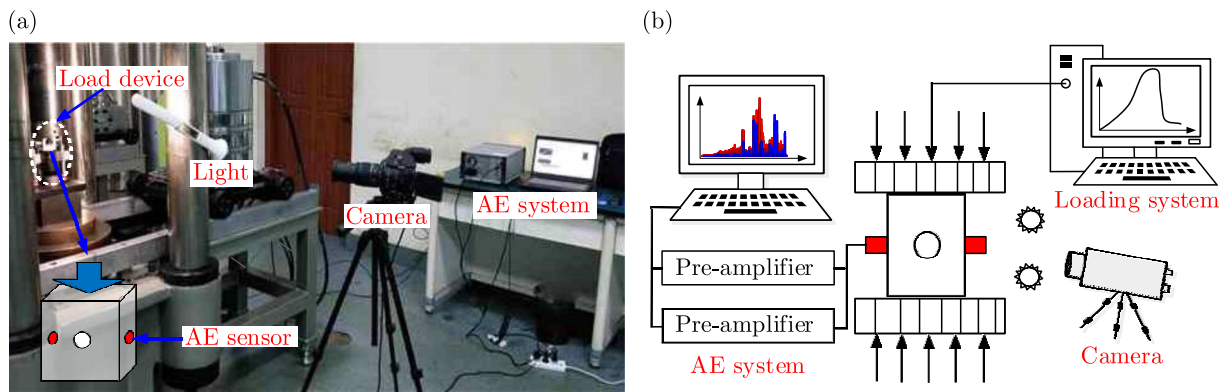


Fig. 2. Experimental system: (a) test system layout, (b) schematic diagram

two non-loading surfaces on the left and right sides of the sample. The sensor layout and loading methods are shown in Fig. 2b. Images of the excavation hole destruction process were obtained by the visual observation system, and the entire test process was recorded.

A displacement control method was used in the uniaxial test. Axial pressure was applied at a loading rate of 0.25 mm/min up to specimen fracture while recording data and images by means of acoustic emission. The acoustic emission threshold equaled 40 dB and the sampling frequency was 10 MHz.

3. Results and analysis

3.1. Variation of mechanical parameters

The stress-strain curves of the specimens under five different D/H ratios are shown in Fig. 3a. The peak stress for each specimen size increased as the D/H ratio decreased from 0.6 to 0.24. The opposite was observed when D/H was equal to 0.2. When the D/H ratio decreased to a certain value, the peak stress no longer significantly changed. When the D/H ratio was 0.6, the peak stress was 19.3 MPa. When the D/H ratio was reduced to 0.3, the peak stress increased to 67.2 MPa. When the D/H ratio was 0.24 or 0.2, the peak stress was 81.2 MPa or 79.1 MPa, as shown in Fig. 3b. The aforementioned data demonstrates that when the D/H ratio reaches 0.24, compared to the uniaxial compressive strength of the complete green sandstone, the difference is within 4% and the peak stress is stable; however, owing to the existence of holes, the overall strength was reduced.

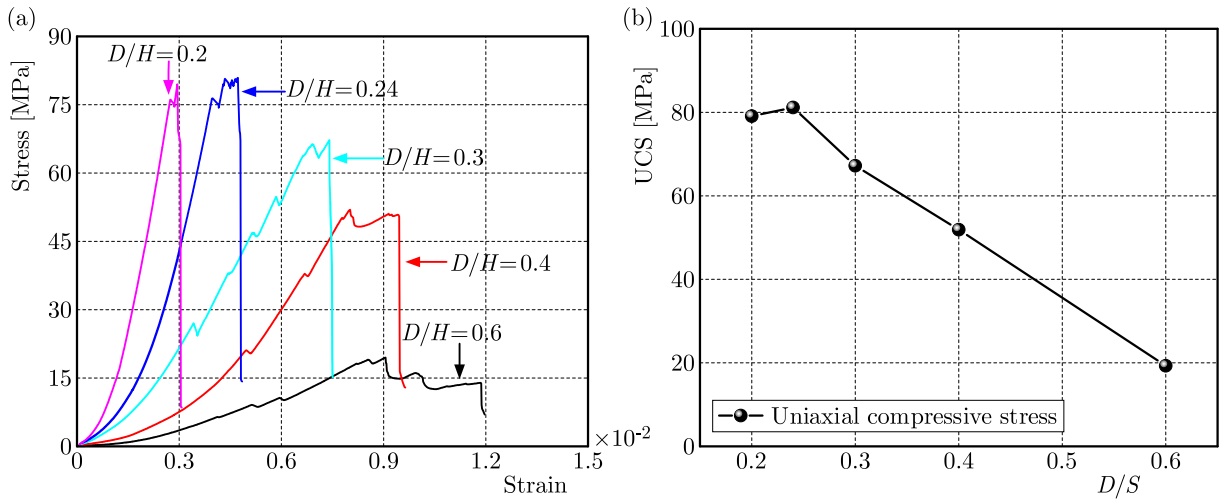


Fig. 3. Stress-strain curve and the UCS of different D/H ratios: (a) stress-strain curve, (b) uniaxial compressive stress

In addition, there were apparent differences in the stress-strain curves for the five D/H ratios. As the D/H ratio decreases, the number of times the stress decreases is gradually reduced, and the stress growth rate gradually increases. For the stress curve before the peak, the D/H value is equal to 0.3 as the threshold value. When the D/H ratio is 0.6 and 0.4, the stress decreases on three occasions in the stress curve, and on five occasions when the D/H value is 0.3. This indicates that when the D/H value is greater than or equal to 0.3, the stress decreases several times and the distribution becomes more uniform. However, when the D/H value is less than 0.3, the number of times the stress decreases is lower and only distributed near the peak. The curves of the D/H ratios of 0.2 and 0.24 both demonstrated a decrease several times near the peak, which is clearly different from the other D/H ratios.

When failure first occurs near a hole, V-shaped breakouts are formed on both sides owing to the stress concentration; however, the specimen remains to have a load-bearing capacity as a whole, and there is no decrease in stress observed in the axial direction. This behaviour is consistent with the findings from previous literature (Si *et al.*, 2018; Gong *et al.*, 2017). Therefore, the main reason for the numerous aforementioned times the stress decreases is the overall rupture of the specimen. When the D/H value is greater than or equal to 0.3, a destruction of the specimen occurs during the stress-loading stage before the peak, and its level is relatively large. When the D/H ratio is 0.24 or 0.2, the loading process was stable in the early stage and there was no main fracture.

3.2. Fracture process of the borehole

Table 2 and Fig. 3 present the relationship between the stress and loading time as well as the corresponding images of the failure process of the five ratio size samples. As shown in Table 2, the number of times the stress decreases is reduced with a decrease in the D/H ratio, and the time of hole failure gradually approaches the time of the stress decrease with a decrease in the D/H ratio. Meanwhile, the degree of hole failure became evident as the D/H ratio decreased.

Table 2. Statistics of hole failure characteristics

D/H	Pre-peak stress drop times	First decrease in stress value	First fracture time of hole	Hole fracture form
0.6	3	161.9	None	Not obvious
0.4	3	218.1	None	Not obvious
0.3	5	198.9	400.5	Slight V-pit
0.24	1	288.8	288.4	Obvious V-pit
0.2	1	254.6	254	Obvious V-pit

As shown in Table 2, when the D/H ratio is greater than or equal to 0.3, stress drop occurs several times in the pre-peak stress curve, but no significant fractures occur in the hole. However, when the D/H ratio is less than or equal to 0.24, the time to fracture and stress decrease are nearly the same.

The following Section provides an analysis based on the data presented in Fig. 4. As shown in Fig. 4a, 4b and 4c, when $D/H = 0.6$, the stress decreases three times in the stress-time curve before the peak. There is no evident change in the hole in the corresponding image record. As shown in Fig. 4a, the extent of cracks above the hole gradually increases. It can be inferred here that the decrease in stress is not related to damage of the hole, but to overall damage of the specimen. When the same D/H value is 0.4, the stress-time curve presents three apparent times of the stress decrease, and then the stress decreases to a lower value; however, the hole does not change during the corresponding time. When the D/H ratio is 0.3, the hole begins to fail. The first decrease in stress and the hole failure occur at 198.9s and 400.5s, respectively. The stress decreases five times in the stress curve; however, the hole completely fails only at the fifth decrease in stress. The aforementioned data demonstrates that when the D/H ratio is less than or equal to 0.3, the specimen appears to be integrally damaged, causing a decrease in the stress; the holes are not apparently damaged at this size ratio.

As shown in Fig. 4d and 4e, when the D/H ratio is 0.24 or 0.2, the entire pre-peak stress-time curve is relatively complete, there are no small decreases in the stress, and the fracture form of the hole is more apparent. Combined with the data in Table 2, it was found that when the decrease in stress occurred close to the time of hole failure, the hole damage gradually became more severe as the stress increased until the rock burst.

3.3. Acoustic emission characteristics

3.3.1. Analysis of AE event counts

Figure 5 presents the stress-time and acoustic emission ringing count curves with five ratios. The ringing count is the number of oscillations in the signal that crosses the threshold. It is a parameter that reflects the intensity and frequency of the acoustic emission activity and can be used to reflect the rupture law inside the sample.

As shown in Fig. 5, the acoustic emission pattern of different specimens is similar to that of the stress-strain curve, indicating that the time of stress reduction corresponds to the peak time of ringing counts. There are also several peaks in the ringing counts in regions where there

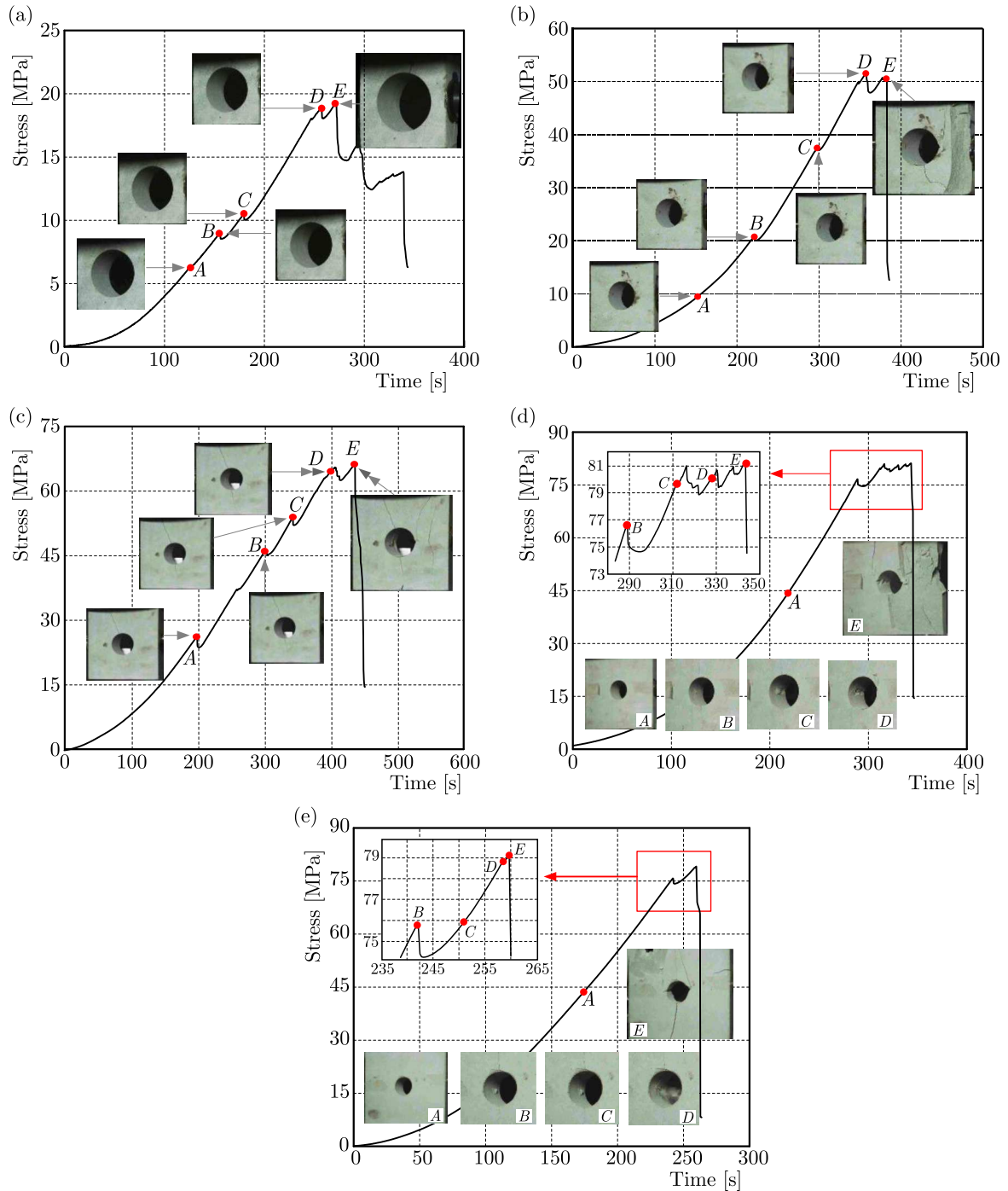


Fig. 4. Failure process of specimens with different D/H ratios: (a) $D/H = 0.6$, (b) $D/H = 0.4$, (c) $D/H = 0.3$, (d) $D/H = 0.24$, (e) $D/H = 0.2$

is no significant stress drop, indicating that the AE is more sensitive to specimen fracture than stress. For example, when the D/H ratio is 0.6, the curve has three distinct stress drop times before it peaks, with distinct ringing counts occurring at the corresponding times.

By combining the data in Figs. 4 and 5, it was found that the rule of hole failure was also consistent with the rule of ringing technology. When the D/H ratio was greater than or equal to 0.3, the ringing count increased several times during the pre-peak period. Based on the decreases in the stress curve and the damage indicated by the image of the hole, it was found

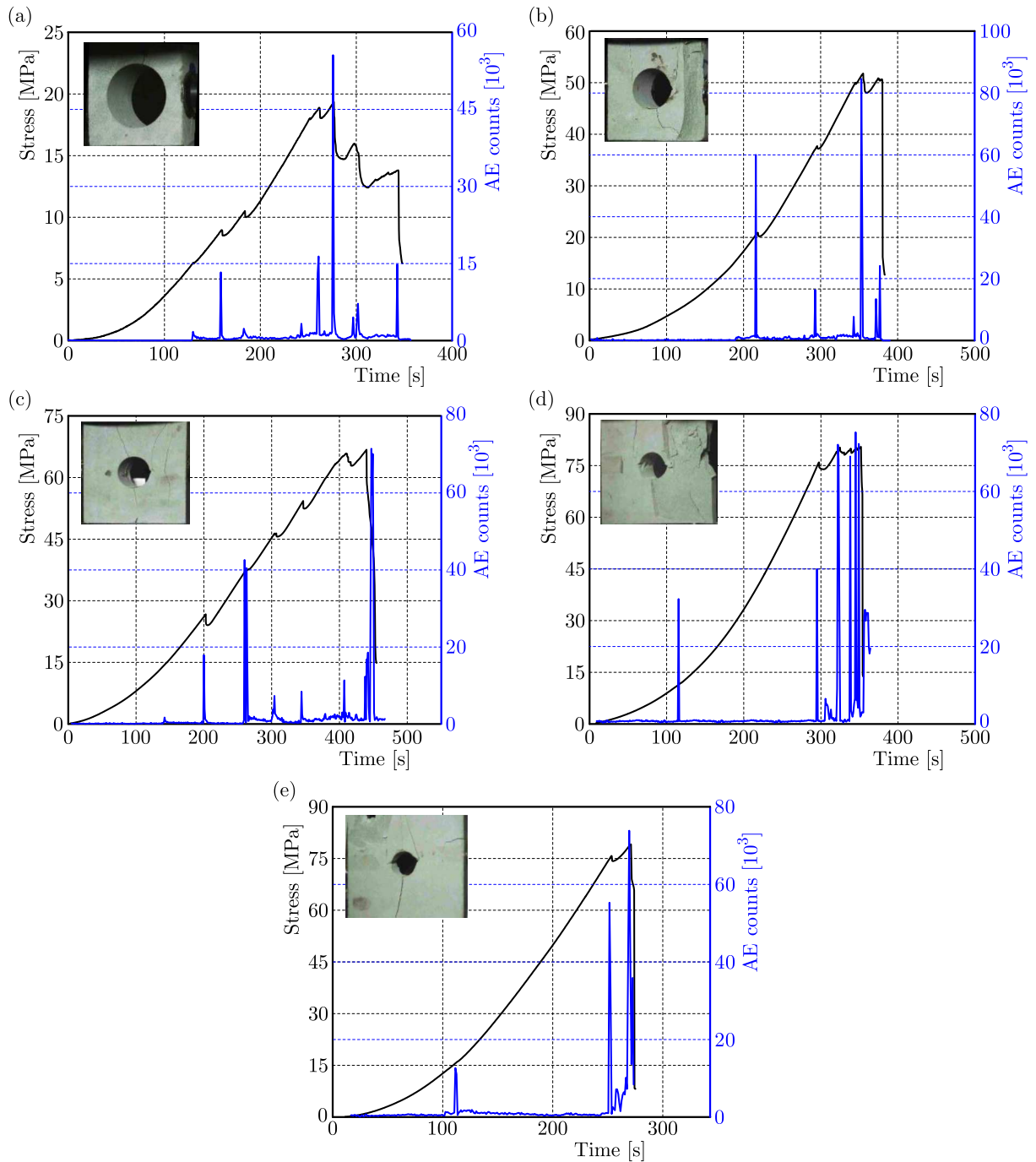


Fig. 5. Stress-time and acoustic emission ringing count curves: (a) $D/H = 0.6$, (b) $D/H = 0.4$, (c) $D/H = 0.3$, (d) $D/H = 0.24$, (e) $D/H = 0.2$

that the peak of the ringing count was mainly owing to the overall damage of the sample, and the hole damage in the entire process was not apparent.

When the D/H ratio was 0.24 and 0.2, the peak of the acoustic emission ringing count was mainly concentrated at the time the first decrease occurred, sufficiently corresponding to the hole failure time, which was manifested as a peak of the ringing count when the hole ruptured. At the same time, these two ratios are different from the hole failure law, and there is a count peak in the two ratios before loading. However, the stress curve and hole do not change.

3.3.2. Analysis of AE energy

The stress-time and acoustic emission energy curves under five sizes of ratios are shown in Fig. 6. They were calculated as the area under the detection envelope of the event signal, including the count rate and total count. The acoustic emission energy rate represents the amount of energy released per unit time during the test, and the cumulative energy is the sum of the released energies. According to the change law of acoustic emission energy, the destruction process can be divided into the three following periods: quiet, development, and outbreak or explosion.

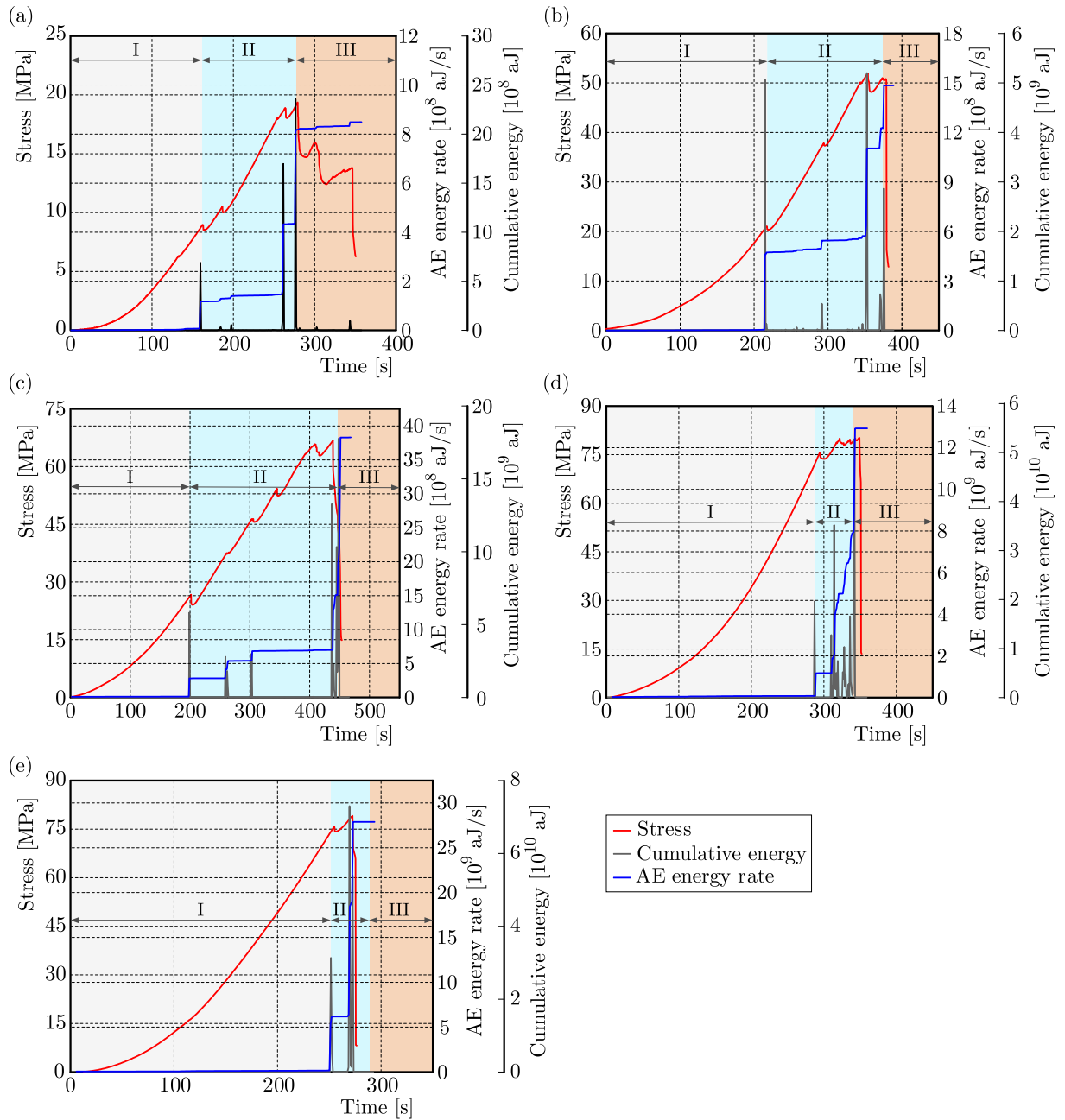


Fig. 6. Stress-time and acoustic emission energy curves: (a) $D/H = 0.6$, (b) $D/H = 0.4$, (c) $D/H = 0.3$, (d) $D/H = 0.24$, (e) $D/H = 0.2$

(1) Quiet period: When the D/H ratio was 0.6, 0.4, or 0.3, the quiet period accounted for approximately 50% of the loading time, and no apparent changes were observed in the hole ground conditions, the entire sample, and the acoustic emission energy rate. The cumulative energy steadily increased, indicating that no energy was released during this period, which was the energy accumulation period. When the D/H ratio was 0.24 or 0.2, the proportion of quiet periods increased to approximately 80%, and the holes and specimens remained unchanged.

(2) Development period: When the D/H ratio was 0.6, 0.4, or 0.3, the specimen demonstrated large cracks, stress drops occurred where the hole damage was not apparent, the acoustic emission energy rate demonstrated a large sudden increase, and the accumulated energy demonstrated a step growth, which indicated the release of energy owing to the overall destruction of the sample. When the D/H ratio was 0.24 or 0.2, the holes were gradually destroyed, the acoustic emission energy rate increased, and the accumulated energy gradually increased in steps, indicating that the hole destruction process was accompanied by an energy release. A low level appeared after the energy rate suddenly increased with the energy rate and the step-like cumulative energy indicating that there was a “short quiet period” of acoustic emission energy.

(3) Explosion period: The specimen had the greatest degree of damage in this period; the stress reached its peak, the acoustic emission energy rate sharply increased, and the cumulative energy increased approximately linearly and reached a maximum. When the D/H ratio was 0.6 or 0.4, macroscopic cracks appeared on the surface of the specimen, but the hole did not show significant V-pit damage. When the D/H ratio was 0.3, 0.24, or 0.2, the specimen was severely destroyed at the hole and, eventually, the whole specimen was destroyed.



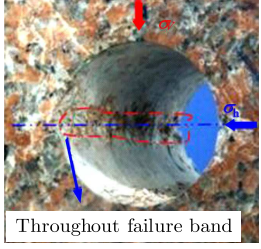
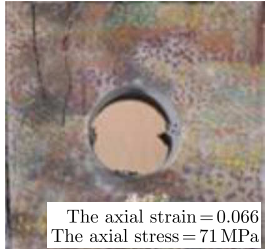
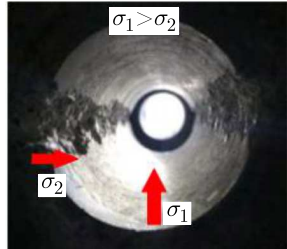
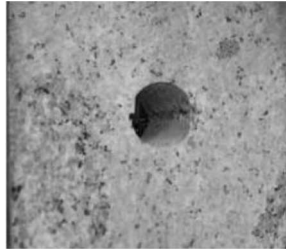
The aforementioned analysis demonstrates that with a decrease in the D/H ratio, the time of the sudden increase in the acoustic emission energy rate gradually shifts back, indicating that the specimen transfers from overall damage to the hole damage. A similar test by Liu and Li (2010) found that the acoustic emission energy was basically unchanged before the hole was destroyed, and the acoustic emission energy rate suddenly increased when the hole began to break. In this study, the same rule was found for samples with D/H ratios of 0.24 and 0.2. At the same time, from the beginning of the hole destruction to the occurrence of rock bursting, there was a short quiet period of acoustic emission energy; after several conversions of the “energy peak-short quiet period”, rock bursting occurred in the sample. This indicates that the “short quiet period” of acoustic emission energy in the development period can be used as a precursor for bursts in the opening.

4. Discussion

4.1. Failure characteristics in different hole tests and the damage mechanism

Table 3 lists the data of the hole fracture form under different D/H ratios. As the D/H ratio decreases from 0.5 to 0.21, the specimens show significant V-shaped pit damage, i.e., red sandstone and granite ($D/H = 5$). V-shaped pits were formed on both sides of the opening wall and it extended along the axial direction of the hole, which is consistent with field observations (Zhang *et al.*, 2012). In this paper, no significant V-shaped pit was exhibited when D/H was greater than 0.3, which may be related to stress conditions. The hole test can be considered as a planar strain problem, ignoring deformation in the axial direction of the hole. When the specimen is under biaxial stress, the horizontal stress increases the overall stability of the specimen, leading to destruction of the hole wall under the maximum tangential stress. Under a uniaxial loading, a specimen with a large D/H ratio corresponds to a larger strain, which can easily lead to an overall splitting damage of the specimen.

Table 3. Comparison of the hole test with different D/H ratios

D/H	0.5	0.5	0.39
Rock type	Red sandstone	Granite	Granite
Loading method	True triaxial (Gong <i>et al.</i> , 2017)	True triaxial (Si <i>et al.</i> , 2018)	Biaxial (Hu <i>et al.</i> , 2019)
Size	100 × 100 × 100 mm	100 × 100 × 100 mm	200 × 20 × 200 mm
Hole failure form	 Overall look	 Maximum principal stress	 Throughout failure band
D/H	0.35	0.3	0.21
Rock type	Marble	Granite	Granite
Loading method	Uniaxial (Liu and Li, 2010)	Biaxial (Liang <i>et al.</i> , 2019)	Biaxial (Zhang <i>et al.</i> , 2016)
Size	100 × 100 × 100 mm	150 × 150 × 150 mm	150 × 150 × 75 mm
Hole failure form	 The axial strain = 0.066 The axial stress = 71 MPa	 $\sigma_1 > \sigma_2$ σ_2 σ_1	

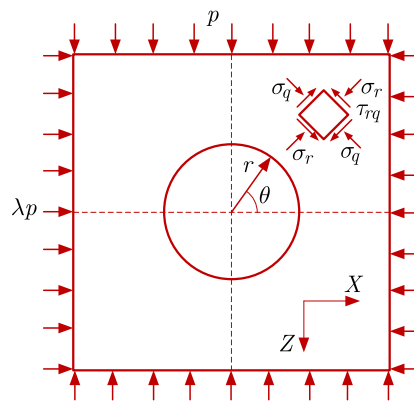


Fig. 7. Tunnel stress calculation model

It is assumed that the rock mass is in a three-way stress state before tunnel excavation, where X and Y are the horizontal, and Z the vertical stress directions. Assuming that the tunnel axial direction is arranged along the Y -direction, the surrounding rock can be regarded as a homogeneous, continuous and isotropic elastomer before damage, and no deformation occurs along the axial direction of the tunnel. Therefore, the problem can be regarded as a planar strain problem and the tunnel stress calculation model can be established as shown in Fig. 7.

By elastic mechanics, the stress in the tunnel rock is

$$\begin{aligned}\sigma_r &= \frac{p}{2} \left[(1 + \lambda) \left(1 - \frac{R^2}{r^2} \right) - (1 - \lambda) \left(1 - 4 \frac{R^2}{r^2} + 3 \frac{R^4}{r^4} \right) \right] \cos(2\theta) \\ \sigma_\theta &= \frac{p}{2} \left[(1 + \lambda) \left(1 + \frac{R^2}{r^2} \right) + (1 - \lambda) \left(1 + 3 \frac{R^4}{r^4} \right) \right] \cos(2\theta) \\ \tau_{r\theta} &= -\frac{p}{2} \left[(1 - \lambda) \left(1 + 2 \frac{R^2}{r^2} - 3 \frac{R^4}{r^4} \right) \right] \sin(2\theta)\end{aligned}\quad (4.1)$$

where p is the vertical stress, λ is the lateral pressure coefficient, σ_r , σ_θ and $\tau_{r\theta}$ are the radial, tangential and shear stresses of the surrounding rock in polar coordinates, respectively, R is the radius of the tunnel excavation, r is the distance from the rock unit to the center of the tunnel and θ is the angle between the rock unit and the horizontal direction.

From Eqs. (4.1), when $r = R$, only tangential stress exists at the tunnel wall, and the maximum tangential stress is located at the midpoint of the two tunnel gangs ($\theta = 0^\circ$). The maximum tangential stress is

$$\sigma_{\theta_{\max}} = (3 - \lambda)p \quad (4.2)$$

When the maximum tangential stress in the tunnel wall exceeds the uniaxial strength of the rock material, the tunnel wall breaks. In the tests in this paper, when D/H was greater than 0.3, the hole wall suffered V-shaped pit damage, indicating that the maximum tangential stress on both sides of the hole exceeded its material strength, leading to failure on both sides of the hole.

4.2. The guiding significance of borehole behaviour

The estimation of the extent of damage is an important aspect in the assessment of underground tunnel and/or roadway stability and its support. Martin *et al.* (1999) calculated the damage range of a circular cavern, and the ratio of the damage range to the radius of the cavern was 1.0-1.5, indicating that the destruction area of the cavern was 1.5 times the excavation radius. The stress in the radial direction of the cavern was distributed in a gradient; the position distant from the cavern gradually reached the original rock stress level, and the surrounding rock gradually reached an undamaged state. There was a transition between the undamaged and damaged areas, called the affected area of damage. This area provides damage energy for the damaged area.

A similar rule was observed in the test in this study, and a certain range was required when a specimen with a fixed hole diameter (30 mm in diameter) failed. Combined with the analysis of the test data in this study, when the D/H ratio was greater than or equal to 0.3, the loading stress curve fluctuated. Visual observations of the hole fracture process confirmed that the integrity of the sample was damaged, and the integrity of the sample damaged the acoustic emission data. Irregular fluctuations occurred when the multiple AE activity peaks occurred during the pre-peak period. When the D/H ratio was less than 0.3, the loading curve stabilized. The video image recordings proved that the first rockburst occurred after the hole fracture, accompanied by acoustic emission activity, indicating that significant hole fracture occurred in the specimen when the D/H ratio was less than 0.3. For a specimen with a fixed hole diameter, the decrease in the D/H ratio was due to an increase in the rock area around the cavern. When the surrounding rock area was small, the hole damage area and the affected area were also small, energy for the hole damage could not be supplied, and stress failure occurred in the entire specimen. When the surrounding rock area was consistent, hole failure required sufficient energy, and the hole first destroyed the specimen and subsequently failed. At the same time, under this test material, the appropriate D/H ratio is 0.4 or 0.2.

5. Conclusions

This study conducted a series of laboratory tests to investigate the failure characteristics of pre-driven openings in rock specimens to better understand the impact of the size factor on the failure process. The main findings are summarized as follows:

- The D/H ratio has a controlling effect on the stress curve, and the overall strength of the specimen decreases with increasing D/H ratios. When the D/H ratio is greater than or equal to 0.3, the stress curve is unstable, and the stress decreases multiple times. When the D/H ratio is less than 0.3, the stress curve is stable without several points of stress reduction.
- The D/H ratio affects the failure pattern of the hole specimen. When the D/H ratio is greater than or equal to 0.3, the hole fracture is not apparent, and the reduction in stress causes the integral fracture of the specimen. When the D/H ratio is less than 0.3, V-shaped pit occurs in the hole, and the hole degradation precedes the overall failure of the specimen.
- The AE evolution characteristics of the hole specimen with different D/H ratios can be categorized into three stages: quiet, development, and explosive. When the D/H ratio is 0.24 or 0.2, the “short quiet period” of AE energy can be used as a precursor for rock bursts.

The results of this study can provide a reference for determining the extent of failure of underground openings. Future studies should consider different loading environments and variations in the specimen size.

Acknowledgements

The research described in this paper was financially supported by Taishan Scholar Engineering Construction Fund of Shandong Province of China (No. tsqn201812071), National Natural Science Foundation of China (No. 52274086), the Major Program of Shandong Provincial Natural Science Foundation (No. ZR2019ZD13), and Education System government-sponsored study-abroad program of Shandong Province.

References

1. BARANOWSKI P., KUCEWICZ M., PYTLIK M., MAŁACHOWSKI J., 2022, Shock-induced fracture of dolomite rock in small-scale blast tests, *Journal of Rock Mechanics and Geotechnical Engineering*, **14**, 6, 1823-1835
2. CHEN L.X., GUO W.Y., JIANG Y.J., TAN Y., ZHANG Y.Y., LU D., HAN F., 2023, Experimental study on influence of lithology on directional propagation law of type-I cracks, *Journal of Central South University*, DOI: 10.1007/s11771-023-5371-z
3. CHEN L.X., GUO W.Y., ZHANG D.X., ZHAO T.B., 2022, Experimental study on the influence of prefabricated fissure size on the directional propagation law of rock type-I crack, *International Journal of Rock Mechanics and Mining Sciences*, **160**, 105274
4. DONG L., CHEN Y., SUN D., ZHANG Y., 2021, Implications for rock instability precursors and principal stress direction from rock acoustic experiments, *International Journal of Mining Science and Technology*, **31**, 5, 789-798
5. FARADONBEH R.S., TAHERI A., RIBEIRO E.S., KARAKUS M., 2020, Rockburst assessment in deep geotechnical conditions using true-triaxial tests and data-driven approaches, *International Journal of Rock Mechanics and Mining Sciences*, **128**, 104279

6. FARHADIAN H., 2021, A new empirical chart for rockburst analysis in tunnelling: Tunnel rockburst classification (TRC), *International Journal of Mining Science and Technology*, **31**, 4, 603-610
7. GONG F.Q., LUO Y., SI X.F., LI X.B., 2017, Experimental modelling on rock burst in deep hard rock circular tunnels, *Chinese Journal of Rock Mechanics and Engineering*, **36**, 7, 1634-1648
8. HE M.C., JIA X., COLI M., LIVI E., SOUSA L., 2012, Experimental study of rockbursts in underground quarrying of Carrara marble, *International Journal of Rock Mechanics and Mining Sciences*, **52**, 1-8
9. HU X., SU G., CHEN G., MEI S., FENG X., MEI G., HUANG X., 2019, Experiment on rockbursts process of borehole and its acoustic emission characteristics, *Rock Mechanics and Rock Engineering*, **52**, 3, 783-802
10. HUANG L., SI X., LI X., GONG F., LUO Y., 2022, Influence of maximum principal stress direction on the failure process and characteristics of D-shaped tunnels, *International Journal of Mining Science and Technology*, **32**, 5, 1125-1143
11. KUCEWICZ M., BARANOWSKI P., MAZURKIEWICZ Ł., MAŁACHOWSKI J., 2023, Comparison of selected blasting constitutive models for reproducing the dynamic fragmentation of rock, *International Journal of Impact Engineering*, **173**, 104484
12. LIANG P., ZHANG Y.B., TIAN B.Z., YAO X.L., SUN L., LIU X.X., 2019, Experimental study on energy evolution characteristics in the process of tunnel rock burst, *Chinese Journal of Rock Mechanics and Engineering*, **38**, 4, 736-746
13. LIU D., LING K., LI D., HE M., LI J., HAN Z., ZHANG S., 2021, Evolution of anisotropy during sandstone rockburst process under double-faces unloading, *Journal of Central South University*, **28**, 8, 2472-2484
14. LIU Z.W., LI Y.H., 2010, Experimental investigation on the deformation and crack behavior of rock specimen with a hole undergoing uniaxial compressive load, *Engineering Mechanics*, **27**, 8, 133-139
15. LUO Y., GONG F., LIU D., WANG S., SI X., 2019, Experimental simulation analysis of the process and failure characteristics of spalling in D-shaped tunnels under true-triaxial loading conditions, *Tunnelling and Underground Space Technology Incorporating Trenchless Technology Research*, **90**, 42-61
16. MARTIN C.D., 1997, Seventeenth Canadian Geotechnical Colloquium: The effect of cohesion loss and stress path on brittle rock strength, *Canadian Geotechnical Journal*, **34**, 5, 698-725
17. MARTIN C.D., KAISER P.K., MCCREATH D.R., 1999, Hoek-Brown parameters for predicting the depth of brittle failure around tunnels, *Canadian Geotechnical Journal*, **36**, 1, 136-151
18. SI X.F., GONG F.Q., LUO Y., LI X., 2018, Experimental simulation on rockburst process of deep three-dimensional circular cavern, *Rock and Soil Mechanics*, **39**, 2, 621-634
19. SU G., JIANG J., FENG X., JIANG Q., CHEN Z., MO J., 2019, Influence of loading rate on strainburst: an experimental study, *Bulletin of Engineering Geology and the Environment*, **78**, 5, 3559-3573
20. SU G., ZHAI S., JIANG J., ZHANG G., YAN L., 2017, Influence of radial stress gradient on strainbursts: An experimental study, *Rock Mechanics and Rock Engineering*, **50**, 10, 2659-2676
21. WU H., KULATILAKE P., ZHAO G., LIANG W., WANG E., 2019, A comprehensive study of fracture evolution of brittle rock containing an inverted U-shaped cavity under uniaxial compression, *Computers and Geotechnics*, **116**, 1-16
22. ZHANG C., FENG X.T., ZHOU H., QIU S., WU W., 2012, Case histories of four extremely intense rockbursts in deep tunnels, *Rock Mechanics and Rock Engineering*, **45**, 3, 275-288
23. ZHANG W., GUO W., WANG Z., 2022, Influence of lateral pressure on mechanical behavior of different rock types under biaxial compression, *Journal of Central South University*, **29**, 11, 3695-3705

24. ZHANG Y.B., LI J., LIU X.X., TIAN B., 2016, Experimental study of influence of lateral pressure on the characteristics of acoustic emission and damage during the rock burst of tunnel, *Chinese Journal of Underground Space and Engineering*, **12**, 5, 1192-1197
25. ZHAO T.B., XING M.L., GUO W.Y., WANG C.W., WANG B., 2021, Anchoring effect and energy-absorbing support mechanism of large deformation bolt, *Journal of Central South University*, **28**, 2, 572-581

Manuscript received April 10, 2023; accepted for print September 6, 2023